Selective area epitaxy of PbTe-Pb hybrid nanowires on a lattice-matched substrate

Yuying Jiang,[1,*] Shuai Yang,[2,*] Lin Li,[2,*] Wenyu Song,[1,*] Wentao Miao,[1,*] Bingbing Tong,[2] Zuhan Geng,[1] Yichun Gao,[1] Ruidong Li,[1] Fangting Chen,[1] Qinghua Zhang,[3] Fanqi Meng,[3] Lin Gu,[3] Kejing Zhu,[2] Yunyi Zang,[2] Runan Shang,[2] Zhan Cao,[2] Xiao Feng,[1,2,4] Qi-Kun Xue,[1,2,4,5] Dong E. Liu,[1,2,4] Hao Zhang,[1,2,4,†] and Ke He[1,2,4,‡]

[1]*State Key Laboratory of Low Dimensional Quantum Physics, Department of Physics, Tsinghua University, Beijing 100084, China*

[2]*Beijing Academy of Quantum Information Sciences, Beijing 100193, China*

[3]*Institute of Physics, Chinese Academy of Sciences, Beijing 100190, China*

[4]*Frontier Science Center for Quantum Information, Beijing 100084, China*

[5]*Southern University of Science and Technology, Shenzhen 518055, China*

(Received 10 November 2021; accepted 7 March 2022; published 23 March 2022)

Topological quantum computing is based on the braiding of Majorana zero modes encoding topological qubits. A promising candidate platform for Majorana zero modes is semiconductor-superconductor hybrid nanowires. The realization of topological qubits and braiding operations requires scalable and disorder-free nanowire networks. Selective area growth of in-plane InAs and InSb nanowires, together with shadow-wall growth of superconductor structures, have demonstrated this scalability by achieving various network structures. However, the noticeable lattice mismatch at the nanowire-substrate interface, acting as a disorder source, imposes a serious obstacle along with this road map. Here, combining selective area and shadow-wall growth, we demonstrate the fabrication of PbTe-Pb hybrid nanowires—another potentially promising Majorana system—on a nearly perfectly lattice-matched substrate CdTe, all done in one molecular beam epitaxy chamber. Transmission electron microscopy shows the single-crystal nature of the PbTe nanowire and its atomically sharp and clean interfaces to the CdTe substrate and Pb overlayer, without noticeable interdiffusion or strain. The nearly ideal interface condition, together with the strong screening of charge impurities due to the large dielectric constant of PbTe, holds promise towards a clean nanowire system to study Majorana zero modes and topological quantum computing.

DOI: 10.1103/PhysRevMaterials.6.034205

I. INTRODUCTION

Majorana zero modes (MZMs) [1,2] have attracted enormous interest in the past decade for their non-Abelian statistics and potential applications in topological quantum computing (TQC) [3,4]. As a promising platform to realize MZMs and TQC [5,6], semiconductor-superconductor hybrid nanowires have been extensively studied since 2010 with sustained efforts from theory prediction to material growth, device fabrication, and transport measurement, mostly in InAs- and InSb-based systems [7–9]. Guided by theory [10,11] and enabled by material growth [12,13], electron transport experiments on hybrid nanowires have been significantly advanced [14–21] where to date, however, an unambiguous demonstration of MZMs is still lacking. Recent theory developments point out that disorder, even after years of optimization for ballistic transport [22–24], still plays a major role in currently the best InAs/InSb hybrid nanowire devices [25–28]. One solution to the problem is to switch to superconductors with larger superconducting gaps, e.g., Pb [29] and Sn [30], which presumably have a higher tolerance of disorder than the commonly used Al. Another solution, seemingly more difficult, is to replace InAs/InSb with another semiconductor less influenced by disorder [31–33].

In this paper, we demonstrate the molecular beam epitaxy (MBE) growth of PbTe-Pb hybrid nanowires, a promising material candidate for a Majorana search with improvement in both the superconductor and semiconductor respects. PbTe is a IV-VI semiconductor with strong spin-orbit coupling and a band gap and Lander g factor similar to InAs/InSb. The ultralarge dielectric constant of PbTe, two orders of magnitude higher than InAs and InSb, can significantly screen charge disorder [34]. Early experiments on PbTe-based two dimensional electron gas have shown ballistic transport [35–38], quantum Hall effect [39–42], and mobility larger than 2×10^5 cm^2/V s [42]. Lead can induce a proximity superconducting gap in PbTe-family materials much larger than Al in InAs/InSb [43,44]. Isolated MZMs are predicted to appear in PbTe-Pb nanowires with the valley degeneracy of PbTe lifted by certain crystalline orientations and device geometries [34].

Moreover, one can find an ideal substrate—CdTe—for selective area growth (SAG) of in-plane epitaxial PbTe nanowires and networks. Previously reported SAG InAs [45–50] and InSb [51–53] nanowires, though demonstrating the scalability needed for future braiding circuits, suffer from the lack of lattice-matched substrates. The lattice mismatch, as a serious disorder source, significantly reduces the quality of

*These authors contributed equally to this work.
†hzquantum@mail.tsinghua.edu.cn
‡kehe@tsinghua.edu.cn

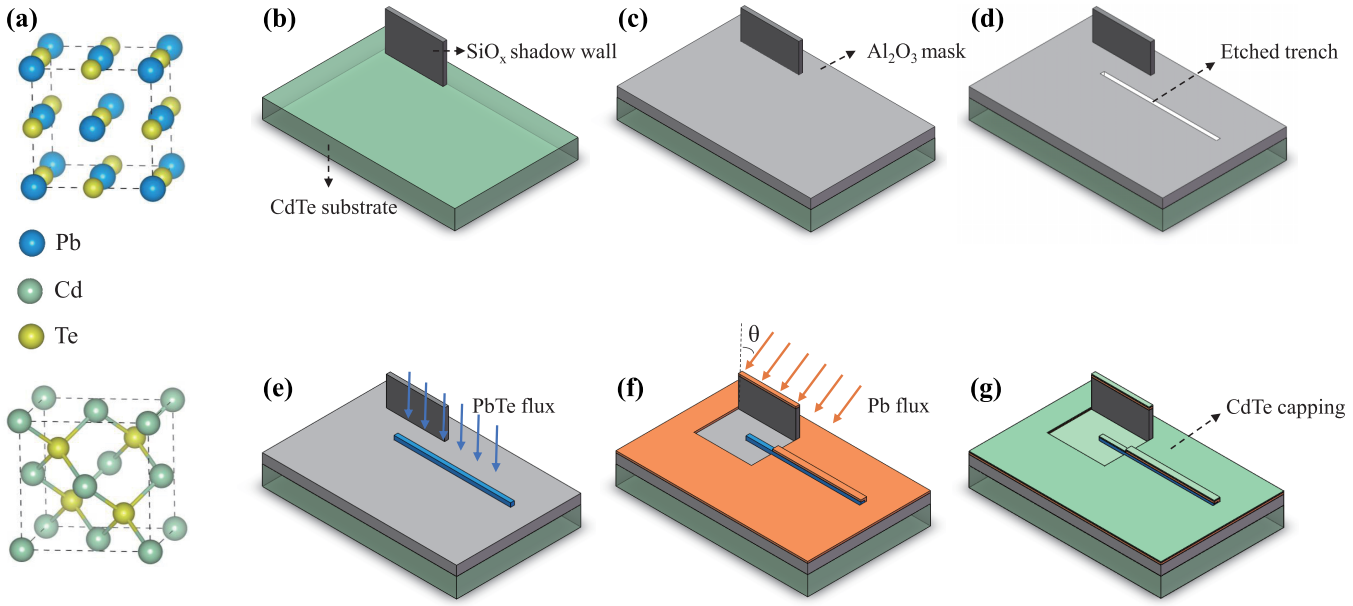

FIG. 1. Schematic crystal structures of PbTe and CdTe and fabrication procedure of prepatterned CdTe substrates and PbTe-Pb hybrid nanowires. (a) Crystal structures of PbTe and CdTe. (b) Preparation of SiO_x shadow walls (dark grey) on a CdTe substrate (green). (c) Al_2O_3 mask (light grey) deposition. (d) Wet etching of Al_2O_3 with openings on a CdTe substrate (white). (e) Selective area growth of PbTe nanowires (blue). The arrows represent the PbTe flux direction. (f) Shadow wall growth of Pb overlayer (orange). The arrows represent Pb flux direction. (g) Capping the device with CdTe.

SAG nanowires and is considered as the biggest barrier for the SAG approach to scalable topological quantum computing. CdTe is a commonly used substrate for growing II-VI and IV-VI semiconductors with a band gap of 1.5 eV and type I band alignment with PbTe. PbTe and CdTe have nearly identical lattice constants but distinct crystalline structures [rocksalt for PbTe and zinc blende for CdTe, as shown in the schematic lattice structures in Fig. 1(a)], which minimizes both the strain and intermixing in their heterostructures [54,55]. Therefore, the PbTe nanowires epitaxied on CdTe substrates are expected to show an ideal interface.

In this study, we not only grow epitaxial PbTe nanowires on CdTe substrates with SAG, but also *in situ* prepare Pb nanostructures on the PbTe nanowires using shadow-wall growth in the same MBE chamber [24,56–59], avoiding the uncontrollable Pb etching process that may deteriorate the device quality. Our results provide a complete toolbox of fabricating scalable topological quantum computation devices with a new (potentially better) hybrid nanowire system for Majorana detection.

II. EXPERIMENT

Figures 1(b)–1(g) show the fabrication/growth sequence schematic of the PbTe-Pb hybrid nanowires. We start with a commercial CdTe(001) substrate [green in Fig. 1(b)] on which silicon oxide (SiO_x) shadow walls (dark grey) are fabricated by electron beam lithography (EBL); see Fig. S1 in the Supplemental Material for details [60]. The shadow walls, 500–700 nm high, are made from inorganic negative resist Hydrogen SilsesQuioxane (HSQ) which is converted into SiO_x after electron beam exposure. A 20–40-nm-thick Al_2O_3 mask layer [light grey in Fig. 1(c)] is then uniformly deposited by magnetron sputtering, followed by a wet etching, using Transene Etchant Type D, to open nanowire-shaped trenches [white line in Fig. 1(d)] for SAG. After cleaning by oxygen plasma, the prepatterned substrates are loaded into the MBE chamber (Omicron Lab-10), in which they are further treated by Ar^+ sputtering and annealing at 280 °C until a clean CdTe surface at the mask openings is obtained.

PbTe nanowires are grown with a PbTe compound source (99.999%) evaporated by a standard Knudson cell with the beam flux ∼1.24 ML/min. Selective growth of PbTe on the exposed CdTe surface at the mask openings is achieved [Fig. 1(e)] when the substrate temperature (T_{subs}) is between ∼310 and ∼340 °C. To grow Pb nanostructures on the SAG PbTe nanowires, the sample is *in situ* transferred to another sample stage in the same MBE chamber. Here, the sample is cooled to ∼100 K with liquid nitrogen, as required by 2D growth of Pb films, and tilted such that the angle between the incident Pb flux and sample surface normal direction is 54–61°. Such an evaporation geometry and the 500–700-nm-high shadow walls result in a Pb film with 1–1.3-μm-long shadows grown on the substrate [Fig. 1(f)]. A CdTe capping layer [Fig. 1(g)] is grown to cover the nanowire sample before it is taken out for further fabrications and measurements.

III. RESULTS AND DISCUSSION

A. SEM characterization

Figure 2(a) shows the scanning electron microscope (SEM) image of a PbTe nanowire (along the [010] direction) grown on a CdTe substrate without shadow walls. The nanowire is uniform with a flat surface and nearly straight edges with the length exceeding 7 μm and the width below 200 nm. The atomic force microscope (AFM) image on the surface of such

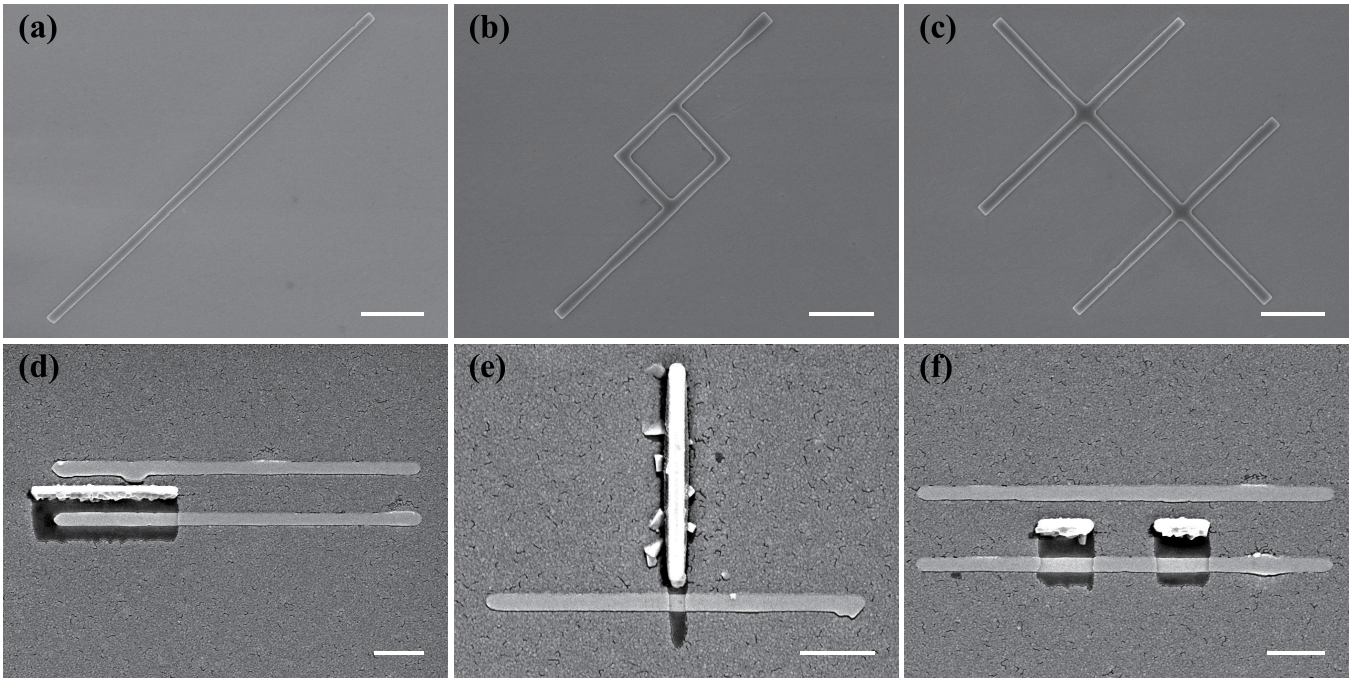

FIG. 2. Scanning electron microscope (SEM) images of PbTe and PbTe-Pb nanowires and nanostructures grown on CdTe(001). (a)–(c) SEM images of a PbTe nanowire (a), an Aharonov-Bohm loop (b), and a double cross (Hall bar) composed of PbTe nanowire (c), all selectively grown on CdTe (001). (d)–(f) SEM images of PbTe-Pb hybrid nanowire structures for NS tunneling spectroscopy (d), SS Josephson junction (e), and superconducting island devices (f), respectively. All the scales bars are 1 micron.

a nanowire (see Fig. S2 in the Supplemental Material [60]) shows atomically flat terraces spaced by ∼3.23 Å high steps, corresponding to the interlayer spacing of PbTe (001). The step-terrace structure is typical of an epitaxial film on a single crystal substrate. More complex nanowire-based structures are obtained in mask openings of different shapes, such as the loop shown in Fig. 2(b) and the double crosses shown in Fig. 2(c), both composed of nanowires of ⟨100⟩ directions. The two kinds of structures can be used in future Aharonov-Bohm (AB) effect and Hall effect experiments, respectively. These structures share the same uniformity as the nanowires without obvious faceting observed at crossings and corners, because {001} family surfaces of rocksalt crystals have the lowest surface energy. PbTe nanowires along ⟨110⟩ directions with similar uniformity can also be obtained, though requiring more careful tuning of the growth parameters. Faceted edges appear in the nanowires along other directions (see Fig. S3 in the Supplemental Material [60]).

Figures 2(d)–2(f) display the SEM images of three different PbTe-Pb in-plane junctions prepared by shadow-wall growth of Pb on SAG PbTe nanowires (along the [110] direction). The three structures, made by different positions of shadow walls (the bars with the brightest colors) relative to PbTe nanowires, correspond to N-S, S-S, and N-S(island)-N devices, respectively (N for normal metal and S for superconductor). N-S devices can be used for tunneling spectroscopy to study the induced superconducting gap and Majorana or Andreev subgap states. S-S devices are for Josephson junctions while N-S(island)-N devices are for studies of "Majorana island." The Pb overlayers grown on PbTe nanowire are atomically flat as shown in the AFM image (see Fig. S2 in the Supplemental Material [60]). On the Al_2O_3 mask, the Pb layer is much rougher, as a result of the merging of three-dimensional (3D) Pb islands with different crystalline orientations. The edges of the Pb overlayers on the PbTe surface are very abrupt, making nearly ideal termination of the superconducting region hosting MZMs.

B. TEM characterization

High-resolution scanning transmission electron microscopy (STEM) was used to characterize the cross-sectional structure of a PbTe-Pb hybrid nanowire along the [110] direction (a 56-nm-thick PbTe nanowire with a 16–18-nm-thick Pb film and a 10-nm CdTe capping layer). Fig. 3(a) shows the high-angle annular dark field (HAADF) image, from which the CdTe substrate, the PbTe wire, the Pb overlayer, and the CdTe capping layer are clearly distinguished. The PbTe wire is partly grown in the trench of CdTe substrate etched by Ar^+ sputtering and partly overgrown out of the Al_2O_3 mask. The overgrowth can be controlled by adjusting the growth time. The Pb overlayer becomes blurred at the edges, presumably broken up by the focused ion beam (FIB) process during the TEM sample preparation (note that the top CdTe capping layer is intact, suggesting that the breakup of the Pb layer occurred after the growth was completed). Despite these imperfections, the interfaces between neighboring layers are rather sharp, suggesting little interlayer diffusion. It is further confirmed by the energy-dispersive x-ray spectroscopy (EDX) maps of Pb, Cd, and Te in Figs. 3(b)–3(d), respectively. The characteristic signals of each element change abruptly across the interfaces to neighboring layers (see Fig. S4 in the Supplemental Material [60]). The atomically resolved STEM images

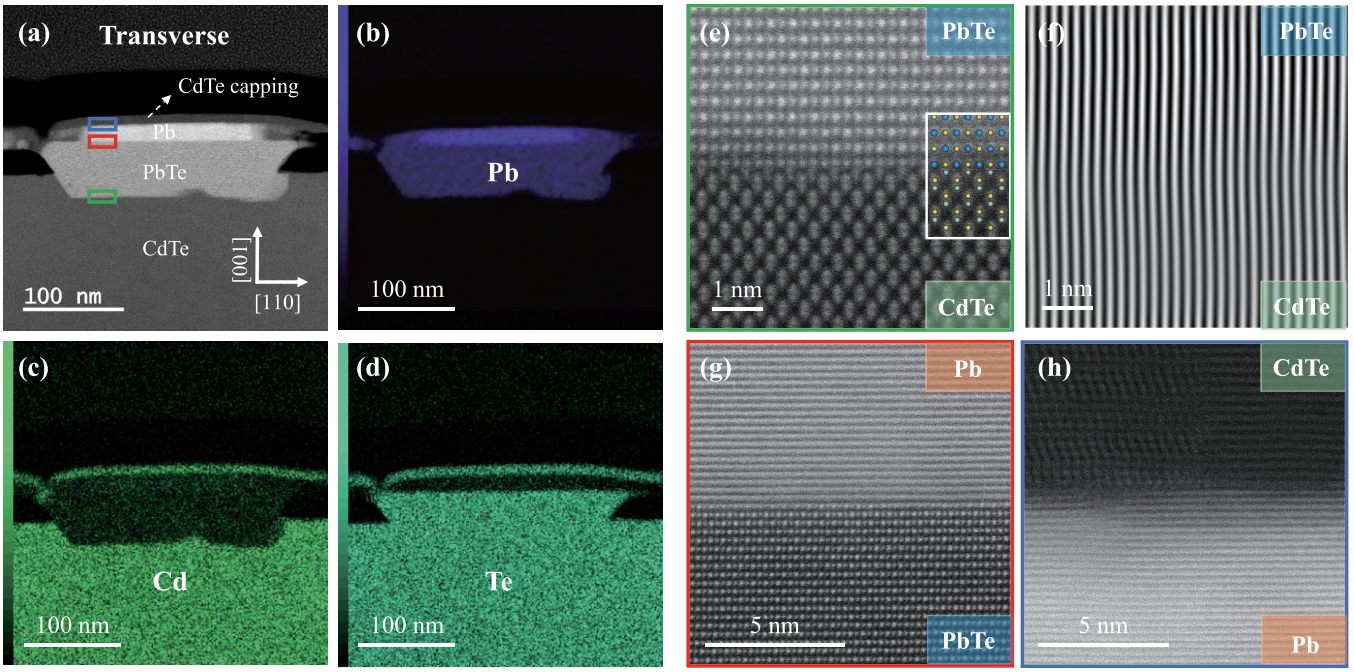

FIG. 3. Scanning transmission electron microscopy characterizations of the cross section of a PbTe-Pb hybrid nanowire grown on CdTe(001) substrate. (a) High-angle annular dark field (HAADF) image. (b)–(d) Energy-dispersive x-ray spectroscopy (EDX) maps of Pb (b), Cd (c), and Te (d), respectively. (e) Atomically resolved image near the CdTe-PbTe interface. (f) Inverse fast Fourier transformation (IFFT) of (e), resolving the columns of atoms as vertical lines. (g), (h) Atomically resolved images near the PbTe-Pb interface (g) and CdTe capping layer-Pb interface (h).

around the CdTe-PbTe interface is shown in Figs. 3(e), S5, and S6 [60]. The PbTe nanowire is nearly perfectly epitaxial on the CdTe substrate with an atomically abrupt interface. From the inverse fast Fourier transformation (IFFT) of the TEM image in Figs. 3(f) and S5 [60], we observe no misfit dislocation which widely exists in InSb-InP and InAs-InP interfaces in early works. The PbTe-Pb interface is also atomically sharp as shown in Fig. 3(g). From the measured interlayer spacing of ∼2.85 Å, we conclude that the Pb overlayer is (111) oriented. The formation of the (111) oriented Pb layer on PbTe(001) surface is due to the low surface energy of Pb(111) surface and the weak bonding between PbTe and Pb. The different surface symmetries rule out any epitaxial relationship between the PbTe(001) nanowire and the Pb(111) overlayer. Nevertheless, no grain boundaries are resolved in the Pb(111) overlayer, suggesting that the size of Pb grains is at least larger than the width of the nanowire. The CdTe capping layer grown on the Pb layer is multicrystalline [Fig. 3(h)], but it also forms an atomically abrupt interface with the Pb layer.

C. Transport properties

In Fig. 4, we display the preliminary electron transport characterization of a SAG PbTe device. Figure 4(a) shows the device SEM image: a PbTe nanowire is contacted by two normal metal electrodes (Ti/Au) after a short *in situ* Ar plasma etching for Ohmic contacts. The channel length (contact spacing) of the device is ∼2.8 μm, long enough for diffusive electron transport. After the measurement, the device was further cut for TEM and EDX analysis (see Fig. S7 in the Supplemental Material [60]) with its cross section shown in Fig. 4(b). Figure 4(c) shows the device conductance tuned by voltage applied to a top gate (V_{TG}). The channel can be fully pinched off and opened as a field-effect transistor. We notice a sizable hysteresis of the pinch off curves for different V_{TG} sweeping directions, which will be discussed below. For the upward sweeping, we can fit the curve to extract the device mobility based on the formula [22,61–63] $G(V_{TG}) = (R_c + \frac{L^2}{\mu C(V_{TG}-V_{th})})^{-1}$, with L representing channel length, μ carrier mobility, V_{th} threshold voltage, R_C the series resistance, and C gate-nanowire capacitance. A key parameter of the fitting is the capacitance C, which we estimate to be 0.709 fF based on a Laplace solver using finite element method by taking the device geometry [Fig. 4(b)] as an input [22]. Quantum confinement effect is also considered which further reduces the capacitance by ∼20% [64]. The fitting curve (red line) shows reasonable agreement with the data (black) with an extracted field effect mobility $\sim 1.5 \times 10^4$ cm^2/V s. This value is significantly (two orders of magnitude) larger than those previously reported in PbTe nanowires [65,66] and slightly lower (the same order of magnitude) than those of the best InSb nanowires [22]. During the growth of this device, the PbTe nanowire was capped by CdTe (see Fig. S7 in the Supplemental Material [60]) to protect the device from possible surface disorder. Without this capping layer (see Fig. S8 in the Supplemental Material [60]), the device mobility is significantly reduced (by roughly an order of magnitude), suggesting the necessity of lattice-matched capping for high quality devices. For the downward sweeping curve, we could not find a reasonable fit using this mobility model. The sizable hysteresis between the upward and downward sweepings can

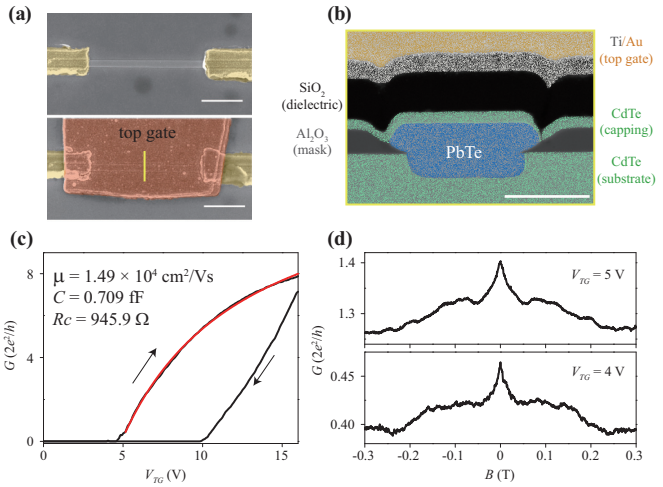

FIG. 4. Basic transport characterization of PbTe nanowires. (a) False-color SEM of a field effect mobility device (device A). For clarity, the upper (lower) panel is the device without (with) dielectric and top gate (orange). Scale bar is 1 micron. (b) Cross section of the device [after measurement, cut along the yellow line in (a)] with each layer labeled. Scale bar is 100 nm. (c) Conductance of the device as a function of top gate voltage (V_{TG}). The arrows indicate V_{TG} sweep directions. The red line is the mobility fitting curve. (d) Magnetoconductance of the device at two V_{TG} settings, resolving a weak antilocalization peak near $B = 0\,\mathrm{T}$. The magnetic field (B) direction is perpendicular to the substrate plane. All measurements are formed in a dilution fridge with a base temperature ~20 mK.

be reduced by an order of magnitude in devices with contact spacing less than 400 nm, as shown in Fig. S9 [60]. The observation suggests that the strong hysteresis of PbTe is probably related to charge trapping at the PbTe surface which can be removed by the accumulation layer induced by the neighboring metal overlayer [67–69] and therefore should not impose an issue for studies on topological superconductivity. Actually, PbTe is known as an "incipient ferroelectric material" [70]. Such a material may exhibit ferroelectriclike properties at the surface where the environment is different from the bulk and thus trap charges there. Figure 4(d) shows the magnetoconductance of the device where a conductance peak near zero magnetic field indicates the effect of weak antilocalization (WAL), indicating the strong spin-orbit coupling. In InSb nanowires, the spin-orbit coupling strength can be estimated from the WAL data [71]. However, different from InSb, the Fermi surface of PbTe is ellipsoid and the electron effective mass is highly anisotropic: from $0.24m_e$ to $0.024m_e$ for longitudinal ($\langle 111 \rangle$) and transversal directions. In addition, the PbTe bulk band structure has a fourfold valley degeneracy which can be lifted in confined nanowire systems [34]. With all these complicated factors, we cannot give a reliable fitting on the measured WAL curve. Further systematic transport studies and more theoretical effects are needed to quantitatively understand the WAL behaviors in PbTe nanowires.

From the characterization results shown above, we can see that although the ultrahigh-vacuum (UHV) *in situ* fabricated PbTe-Pb devices are still far from perfect, they do solve several key problems of "Majorana nanowires": scalability of nanowire networks, lattice match with the substrate, and atomically abrupt and clean interfaces. Pb grown on PbTe induces a charge accumulation layer [67–69], which guarantees the superconductor proximity effect in it. The large dielectric constant of PbTe is expected to significantly reduce the potential variation induced by charge impurities. The insensitivity to disorder probably explains the mobility of $\sim 10^4\,\mathrm{cm}^2/\mathrm{V\,s}$ achieved in the preliminary devices presented in this work: in total, we have successfully fabricated and measured three mobility devices shown in Figs. 4 and S8 [60] for the first round. With future optimization of growth and device fabrication (e.g., mask uniformity, substrate processing, growth condition, single-nucleation, etc.), we expect higher mobility to be achieved. Actually, a mobility over $10^6\,\mathrm{cm}^2/\mathrm{V\,s}$ has already been reported in PbTe films due to the charge screening effect of the large dielectric constant [72], despite far fewer studies devoted to the material than to III-V semiconductors. Therefore, PbTe nanowires have a big advantage in overcoming the disorder problem, the most formidable one now in the nanowire-based approach to topological quantum computing.

IV. CONCLUSION

In summary, we have successfully prepared various PbTe-Pb hybrid nanowires on lattice-matched CdTe substrates by combining SAG and shadow wall growth in the same MBE chamber. The PbTe nanowires have carrier mobility up to $\sim 10^4\,\mathrm{cm}^2/\mathrm{V\,s}$ and form atomically sharp and clean interfaces with the CdTe substrate and Pb overlayer. With the disorder induced by strain and interfaces significantly suppressed and the impurity charges screened by the large dielectric constant, PbTe-Pb hybrid nanowires provide a clean platform to study MZMs and related physics. The UHV device fabrication techniques of the hybrid PbTe-Pb nanowire system developed in this work pave the road towards scalable and disorder-free Majorana networks and circuits to realize topological qubits and braiding.

ACKNOWLEDGMENTS

This work was supported by the National Natural Science Foundation of China (Grants No. 92065206, No. 11974198, No. 12004040, and No. 51788104), the National Key Research and Development Program of China (Grant No. 2017YFA0303303), and Tsinghua University Initiative Scientific Research Program. We thank L. Kouwenhoven and E. Bakkers for valuable discussions. We also thank H. Ying (School of Integrated Circuits, Tsinghua University) for technical assistance. The raw data of this paper are available [73].

[1] N. Read and D. Green, Paired states of fermions in two dimensions with breaking of parity and time-reversal symmetries and the fractional quantum hall effect, Phys. Rev. B **61**, 10267 (2000).

[2] A. Y. Kitaev, Unpaired majorana fermions in quantum wires, Phys. Usp. **44**, 131 (2001).

[3] A. Y. Kitaev, Fault-tolerant quantum computation by anyons, Ann. Phys. **303**, 2 (2003).

[4] C. Nayak, S. H. Simon, A. Stern, M. Freedman, and S. Das Sarma, Non-abelian anyons and topological quantum computation, Rev. Mod. Phys. **80**, 1083 (2008).

[5] R. M. Lutchyn, J. D. Sau, and S. Das Sarma, Majorana Fermions and a Topological Phase Transition in Semiconductor-Superconductor Heterostructures, Phys. Rev. Lett. **105**, 077001 (2010).

[6] Y. Oreg, G. Refael, and F. von Oppen, Helical Liquids and Majorana Bound States in Quantum Wires, Phys. Rev. Lett. **105**, 177002 (2010).

[7] R. Aguado, Majorana quasiparticles in condensed matter, Riv. Nuovo Cimento **11**, 523 (2017).

[8] R. M. Lutchyn, E. P. A. M. Bakkers, L. P. Kouwenhoven, P. Krogstrup, C. M. Marcus, and Y. Oreg, Majorana zero modes in superconductor–semiconductor heterostructures, Nat. Rev. Mater. **3**, 52 (2018).

[9] E. Prada, P. San-Jose, M. W. A. de Moor, A. Geresdi, E. J. H. Lee, J. Klinovaja, D. Loss, J. Nygård, R. Aguado, and L. P. Kouwenhoven, From andreev to majorana bound states in hybrid superconductor–semiconductor nanowires, Nat. Rev. Phys. **2**, 575 (2020).

[10] T. D. Stanescu, R. M. Lutchyn, and S. Das Sarma, Majorana fermions in semiconductor nanowires, Phys. Rev. B **84**, 144522 (2011).

[11] S. Takei, B. M. Fregoso, H.-Y. Hui, A. M. Lobos, and S. Das Sarma, Soft Superconducting Gap in Semiconductor Majorana Nanowires, Phys. Rev. Lett. **110**, 186803 (2013).

[12] P. Krogstrup, N. L. B. Ziino, W. Chang, S. M. Albrecht, M. H. Madsen, E. Johnson, J. Nygård, C. M. Marcus, and T. S. Jespersen, Epitaxy of semiconductor–superconductor nanowires, Nat. Mater. **14**, 400 (2015).

[13] W. Chang, S. M. Albrecht, T. S. Jespersen, F. Kuemmeth, P. Krogstrup, J. Nygård, and C. M. Marcus, Hard gap in epitaxial semiconductor–superconductor nanowires, Nat. Nanotechnol. **10**, 232 (2015).

[14] V. Mourik, K. Zuo, S. M. Frolov, S. R. Plissard, E. P. A. M. Bakkers, and L. P. Kouwenhoven, Signatures of majorana fermions in hybrid superconductor-semiconductor nanowire devices, Science **336**, 1003 (2012).

[15] M. T. Deng, S. Vaitiekenas, E. B. Hansen, J. Danon, M. Leijnse, K. Flensberg, J. Nygård, P. Krogstrup, and C. M. Marcus, Majorana bound state in a coupled quantum-dot hybrid-nanowire system, Science **354**, 1557 (2016).

[16] S. Albrecht, A. Higginbotham, M. Madsen, F. Kuemmeth, T. Jespersen, J. Nygård, P. Krogstrup, and C. Marcus, Exponential protection of zero modes in majorana islands, Nature (London) **531**, 206 (2016).

[17] H. Zhang, Ö. Gül, S. Conesa-Boj, M. P. Nowak, M. Wimmer, K. Zuo, V. Mourik, F. K. de Vries, J. van Veen, M. W. de Moor, J. D. S. Bommer, D. J. van Woerkom, D. Car, S. R. Plissard, E. P. Bakkers, M. Quintero-Pérez, M. C. Cassidy, S. Koelling, S. Goswami, K. Watanabe *et al.*, Ballistic superconductivity in semiconductor nanowires, Nat. Commun. **8**, 16025 (2017).

[18] Ö. Gül, H. Zhang, J. D. S. Bommer, M. W. A. deMoor, D. Car, S. R. Plissard, E. P. A. M. Bakkers, A. Geresdi, K. Watanabe, T. Taniguchi, and L. P. Kouwenhoven, Ballistic majorana nanowire devices, Nat. Nanotechnol. **13**, 192 (2018).

[19] F. Nichele, A. C. C. Drachmann, A. M. Whiticar, E. C. T. O'Farrell, H. J. Suominen, A. Fornieri, T. Wang, G. C. Gardner, C. Thomas, A. T. Hatke, P. Krogstrup, M. J. Manfra, K. Flensberg, and C. M. Marcus, Scaling of Majorana Zero-Bias Conductance Peaks, Phys. Rev. Lett. **119**, 136803 (2017).

[20] H. Zhang, M. W. A. de Moor, J. D. S. Bommer, D. Xu, G. Wang, N. van Loo, C.-X. Liu, S. Gazibegovic, J. A. Logan, D. Car, R. L. M. Op het Veld, P. J. van Veldhoven, S. Koelling, M. A. Verheijen, M. Pendharkar, D. J. Pennachio, B. Shojaei, J. S. Lee, C. J. Palmstrom, E. P. A. M. Bakkers, S. Das Sarma, and L. P. Kouwenhoven, Large zero bias peaks in InSb-Al hybrid semiconductor-superconductor nanowire devices, arXiv:2101.11456.

[21] H. Song, Z. Zhang, D. Pan, D. Liu, Z. Wang, Z. Cao, L. Liu, L. Wen, D. Liao, R. Zhuo, D. E. Liu, R. Shang, J. Zhao, and H. Zhang, Large zero bias peaks and dips in a four-terminal thin inas-al nanowire device, arXiv:2107.08282.

[22] Ö. Gül, D. J. van Woerkom, I. van Weperen, D. Car, S. R. Plissard, E. P. A. M. Bakkers, and L. P. Kouwenhoven, Towards high mobility insb nanowire devices, Nanotechnology **26**, 215202 (2015).

[23] J. Kammhuber, M. C. Cassidy, H. Zhang, O. Gül, F. Pei, M. W. De Moor, B. Nijholt, K. Watanabe, T. Taniguchi, D. Car *et al.*, Conductance quantization at zero magnetic field in insb nanowires, Nano Lett. **16**, 3482 (2016).

[24] S. Heedt, M. Quintero-Perez, F. Borsoi, A. Fursina, N. van Loo, G. P. Mazur, M. P. Nowak, M. Ammerlaan, K. Li, S. Korneychuk *et al.*, Shadow-wall lithography of ballistic superconductor–semiconductor quantum devices, Nat. Commun. **12**, 4914 (2021).

[25] H. Pan and S. Das Sarma, Physical mechanisms for zero-bias conductance peaks in majorana nanowires, Phys. Rev. Research **2**, 013377 (2020).

[26] S. Das Sarma and H. Pan, Disorder-induced zero-bias peaks in majorana nanowires, Phys. Rev. B **103**, 195158 (2021).

[27] S. Ahn, H. Pan, B. Woods, T. D. Stanescu, and S. Das Sarma, Estimating disorder and its adverse effects in semiconductor majorana nanowires, Phys. Rev. Mater. **5**, 124602 (2021).

[28] B. D. Woods, S. Das Sarma, and T. D. Stanescu, Charge-Impurity Effects in Hybrid Majorana Nanowires, Phys. Rev. Appl. **16**, 054053 (2021).

[29] T. Kanne, M. Marnauza, D. Olsteins, D. J. Carrad, J. E. Sestoft, J. de Bruijckere, L. Zeng, E. Johnson, E. Olsson, K. Grove-Rasmussen *et al.*, Epitaxial Pb on InAs nanowires for quantum devices, Nat. Nanotechnol. **16**, 776 (2021).

[30] M. Pendharkar, B. Zhang, H. Wu, A. Zarassi, P. Zhang, C. Dempsey, J. Lee, S. Harrington, G. Badawy, S. Gazibegovic *et al.*, Parity-Preserving and magnetic field–resilient superconductivity in InSb nanowires with Sn shells, Science **372**, 508 (2021).

[31] M. J. G. Kamphuis, Towards quantum transport in single-crystalline PbTe nanowire MOSFET devices, Master's thesis, Eindhoven University of Technology, 2021.

[32] J. Schlatmann, Josephson junction characterization of PbTe nanowires–towards majorana devices in semiconductor-superconductor hybrid nanowires, Master's thesis, Eindhoven University of Technology, 2021.

[33] S. G. Schellingerhout, E. J. de Jong, M. Gomanko, X. Guan, Y. Jiang, M. S. M. Hoskam, S. Koelling, O. Moutanabbir, M. A. Verheijen, S. M. Frolov *et al.*, Growth of PbTe nanowires by molecular beam epitaxy, Mater. Quantum Technol. **2**, 015001 (2022).

[34] Z. Cao, D. Liu, W.-X. He, X. Liu, K. He, and H. Zhang, Numerical study of PbTe-Pb hybrid nanowires for engineering majorana zero modes, Phys. Rev. B **105**, 085424 (2022).

[35] G. Grabecki, J. Wróbel, T. Dietl, K. Byczuk, E. Papis, E. Kamińska, A. Piotrowska, G. Springholz, M. Pinczolits, and G. Bauer, Quantum ballistic transport in constrictions of n-PbTe, Phys. Rev. B **60**, R5133 (1999).

[36] G. Grabecki, J. Wróbel, T. Dietl, E. Papis, E. Kamińska, A. Piotrowska, A. Ratuszna, G. Springholz, and G. Bauer, Ballistic transport in PbTe-Based nanostructures, Phys. E (Amsterdam, Neth.) **20**, 236 (2004).

[37] G. Grabecki, J. Wróbel, T. Dietl, E. Janik, M. Aleszkiewicz, E. Papis, E. Kamińska, A. Piotrowska, G. Springholz, and G. Bauer, Disorder suppression and precise conductance quantization in constrictions of PbTe quantum wells, Phys. Rev. B **72**, 125332 (2005).

[38] G. Grabecki, J. Wróbel, T. Dietl, E. Janik, M. Aleszkiewicz, E. Papis, E. Kamińska, A. Piotrowska, G. Springholz, and G. Bauer, PbTe–a new medium for quantum ballistic devices, Phys. E (Amsterdam, Neth.) **34**, 560 (2006).

[39] G. Springholz, G. Ihninger, G. Bauer, M. M. Olver, J. Z. Pastalan, S. Romaine, and B. B. Goldberg, Modulation doping and observation of the integral quantum hall effect in $PbTe/Pb_{1-x}Eu_xTe$ multiquantum wells, Appl. Phys. Lett. **63**, 2908 (1993).

[40] M. M. Olver, J. Z. Pastalan, S. E. Romaine, B. B. Goldberg, G. Springholz, G. Ihninger, and G. Bauer, The observation of the integral quantum hall effect in $PbTe/Pb_{1-x}Eu_xTe$ quantum well structures, Solid State Commun. **89**, 693 (1994).

[41] V. A. Chitta, W. Desrat, D. K. Maude, B. A. Piot, N. F. Oliveira Jr., P. H. O. Rappl, A. Y. Ueta, and E. Abramof, Multivalley transport and the integer quantum hall effect in a PbTe quantum well, Phys. Rev. B **72**, 195326 (2005).

[42] V. A. Chitta, W. Desrat, D. K. Maude, B. A. Piot, N. F. Oliveira Jr., P. H. O. Rappl, A. Y. Ueta, and E. Abramof, Integer quantum hall effect in A PbTe quantum well, Phys. E (Amsterdam, Neth.) **34**, 124 (2006).

[43] H. Yang, Y.-Y. Li, T.-T. Liu, H.-Y. Xue, D.-D. Guan, S.-Y. Wang, H. Zheng, C.-H. Liu, L. Fu, and J.-F. Jia, Superconductivity of topological surface states and strong proximity effect in $Sn_{1-x}Pb_xTe$–Pb heterostructures, Adv. Mater. **31**, 1905582 (2019).

[44] H. Yang, Y.-Y. Li, T.-T. Liu, D.-D. Guan, S.-Y. Wang, H. Zheng, C.-H. Liu, L. Fu, and J.-F. Jia, Multiple In-Gap States Induced by Topological Surface States in the Superconducting Topological Crystalline Insulator Heterostructure $Sn_{1-x}Pb_xTe$–Pb, Phys. Rev. Lett. **125**, 136802 (2020).

[45] F. Krizek, J. E. Sestoft, P. Aseev, S. Marti-Sanchez, S. Vaitiekėnas, L. Casparis, S. A. Khan, Y. Liu, T. Stankevič, A. M. Whiticar, A. Fursina, F. Boekhout, R. Koops, E. Uccelli, L. P. Kouwenhoven, C. M. Marcus, J. Arbiol, and P. Krogstrup, Field effect enhancement in buffered quantum nanowire networks, Phys. Rev. Mater. **2**, 093401 (2018).

[46] S. Vaitiekėnas, A. M. Whiticar, M.-T. Deng, F. Krizek, J. E. Sestoft, C. J. Palmstrøm, S. Marti-Sanchez, J. Arbiol, P. Krogstrup, L. Casparis, and C. M. Marcus, Selective-Area-Grown Semiconductor-Superconductor Hybrids: A Basis for Topological Networks, Phys. Rev. Lett. **121**, 147701 (2018).

[47] M. Fahed, L. Desplanque, D. Troadec, G. Patriarche, and X. Wallart, Selective area heteroepitaxy of GaSb on GaAs (001) for in-plane inas nanowire achievement, Nanotechnology **27**, 505301 (2016).

[48] M. Friedl, K. Cerveny, P. Weigele, G. Tütüncüoglu, S. Martí-Sanchez, C. Y. Huang, T. Patlatiuk, H. Potts, Z. Y. Sun, M. O. Hill, L. Güniat, W. Kim, M. Zamani, V. G. Dubrovskii, J. Arbiol, L. J. Lauhon, D. M. Zumbühl, and A. F. i Morral, Template-assisted scalable nanowire networks, Nano Lett. **18**, 2666 (2018).

[49] J. S. Lee, S. Choi, M. Pendharkar, D. J. Pennachio, B. Markman, M. Seas, S. Koelling, M. A. Verheijen, L. Casparis, K. D. Petersson, I. Petkovic, V. Schaller, M. J. W. Rodwell, C. M. Marcus, P. Krogstrup, L. P. Kouwenhoven, E. P. A. M. Bakkers, and C. J. Palmstrøm, Selective-Area Chemical Beam Epitaxy of In-Plane InAs One-Dimensional Channels Grown on InP(001), InP(111)B, and InP(011) Surfaces, Phys. Rev. Mater. **3**, 084606 (2019).

[50] P. Aseev, A. Fursina, F. Boekhout, F. Krizek, J. E. Sestoft, F. Borsoi, S. Heedt, G. Z. Wang, L. Binci, S. Martí-Sanchez, T. Swoboda, R. Koops, E. Uccelli, J. Arbiol, P. Krogstrup, L. P. Kouwenhoven, and P. Caroff, Selectivity map for molecular beam epitaxy of advanced III–V quantum nanowire networks, Nano Lett. **19**, 218 (2019).

[51] L. Desplanque, A. Bucamp, D. Troadec, G. Patriarche, and X. Wallart, In-Plane InSb nanowires grown by selective area molecular beam epitaxy on semi-insulating substrate, Nanotechnology **29**, 305705 (2018).

[52] P. Aseev, G. Wang, L. Binci, A. Singh, S. Martí-. Sánchez, M. Botifoll, L. J. Stek, A. Bordin, J. D. Watson, F. Boekhout *et al.*, Ballistic InSb nanowires and networks via metal-sown selective area growth, Nano. Lett. **19**, 9102 (2019).

[53] R. L. M. Op het Veld, D. Xu, V. Schaller, M. A. Verheijen, S. M. E. Peters, J. Jung, C. Tong, Q. Wang, M. W. A. de Moor, B. Hesselmann *et al.*, In-plane selective area InSb–Al nanowire quantum networks, Commun. Phys **3**, 59 (2020).

[54] W. Heiss, H. Groiss, E. Kaufmann, G. Hesser, M. Boeberl, G. Springholz, F. Schäffler, K. Koike, H. Harada, and M. Yano, Centrosymmetric PbTe/CdTe quantum dots coherently embedded by epitaxial precipitation, Appl. Phys. Lett. **88**, 192109 (2006).

[55] W. Heiss, H. Groiss, E. Kaufmann, G. Hesser, M. Boeberl, G. Springholz, F. Schäffler, R. Leitsmann, F. Bechstedt, K. Koike *et al.*, Quantum dots with coherent interfaces between rocksalt-PbTe and zincblende-CdTe, J. Appl. Phys. **101**, 081723 (2007).

[56] D. J. Carrad, M. Bjergfelt, T. Kanne, M. Aagesen, F. Krizek, E. M. Fiordaliso, E. Johnson, J. Nygård, and T. S. Jespersen, Shadow epitaxy for in situ growth of generic semiconductor/superconductor hybrids, Adv. Mater. **32**, 1908411 (2020).

[57] P. Perla, H. A. Fonseka, P. Zellekens, R. Deacon, Y. Han, J. Kölzer, T. Mörstedt, B. Bennemann, K. Ishibashi, D. Grützmacher *et al.*, Fully In Situ Nb/InAs-Nanowire josephson junctions by selective-area growth and shadow evaporation, Nanoscale. Adv. **3**, 1413 (2021).

[58] S. A. Khan, C. Lampadaris, A. Cui, L. Stampfer, Y. Liu, S. J. Pauka, M. E. Cachaza, E. M. Fiordaliso, J. H. Kang,

S. Korneychuk *et al.*, Highly transparent gatable superconducting shadow junctions, ACS Nano **14**, 14605 (2020).

[59] J. Jung, R. L. Op het Veld, R. Benoist, O. A. van der Molen, C. Manders, M. A. Verheijen, and E. P. Bakkers, Universal platform for scalable semiconductor-superconductornanowire networks, Adv. Funct. Mater. **31**, 2103062 (2021).

[60] See Supplemental Material at http://link.aps.org/supplemental/10.1103/PhysRevMaterials.6.034205 for additional data and analysis.

[61] S. M. Sze, *Physics of Semiconductor Devices* (Wiley, New York, 1981).

[62] R. Martel, T. Schmidt, H. R. Shea, T. Hertel, and P. Avouris, Single- and multi-wall carbon nanotube field-effect transistors, Appl. Phys. Lett. **73**, 2447 (1998).

[63] X. Jiang, Q. Xiong, S. Nam, F. Qian, Y. Li, and C. M. Lieber, InAs/InP Radial Nanowire heterostructures as high electron mobility devices, Nano Lett. **7**, 3214 (2007).

[64] D. Eeltink, Electrostatic simulations of nanowire devices, Master's thesis, Delft University of Technology, 2013.

[65] S. Y. Jang, H. S. Kim, J. Park, M. Jung, J. Kim, S. H. Lee, J. W. Roh, and W. Lee, Transport properties of single-crystalline n-Type semiconducting PbTe nanowires, Nanotechnology **20**, 415204 (2009).

[66] H. Jung, J. H. Lim, F. Xiao, K. H. Lee, Y. H. Choa, B. Yoo, and N. Myung, Electrodeposited single crystalline PbTe nanowires and their transport properties, J. Phys. Chem. Lett. **115**, 2993 (2011).

[67] F. Cerrina, R. R. Daniels, T. X. Zhao, and V. Fano, Interface formation at PbTe(100) surfaces: Ge, Al, and In overlayers, J. Vac. Sci. Technol. B **1**, 570 (1983).

[68] B. Lai, G. M. Wells, F. Cerrina, J. R. Anderson, L. Papagno, and G. J. Lapeyre, Study of interface formation on PbTe, J. Vac. Sci. Technol. A **4**, 977 (1986).

[69] F. Cerrina, R. R. Daniels, and V. Fano, Inversion layers at PbTe interfaces, Appl. Phys. Lett. **43**, 182 (1983).

[70] M. P. Jiang, M. Trigo, I. Savić, S. Fahy, É. D. Murray, C. Bray, J. Clark, T. Henighan, M. Kozina, M. Chollet *et al.*, The origin of incipient ferroelectricity in lead telluride, Nat. Commun. **7**, 12291 (2016).

[71] I. van. Weperen, B. Tarasinski, D. Eeltink, V. S. Pribiag, S. R. Plissard, E. P. A. M. Bakkers, L. P. Kouwenhoven, and M. Wimmer, Spin-orbit interaction in Insb nanowires, Phys. Rev. B. **91**, 201413(R) (2015).

[72] G. Springholz, G. Bauer, and G. Ihninger, MBE of high mobility PbTe films and PbTe/$Pb_{1-x}Eu_xTe$ heterostructures, J. Cryst. Growth **127**, 302 (1993).

[73] http://doi.org/10.5281/zenodo.6135410